Langmuir

Article

pubs.acs.org/Langmuir

Structural Properties of Archaeal Lipid Bilayers: Small-Angle X-ray Scattering and Molecular Dynamics Simulation Study

Andraž Polak,[†] Mounir Tarek,*[,‡,§] Matija Tomšič,[∥] Janez Valant,[⊥] Nataša Poklar Ulrih,[⊥] Andrej Jamnik,[∥] Peter Kramar,[†] and Damijan Miklavčič*[,†]

[†]Faculty of Electrical Engineering, University of Ljubljana, Tržaška cesta 25, SI-1000 Ljubljana, Slovenia

[‡]Université de Lorraine, UMR 7565, F-54506 Vandoeuvre-lès-Nancy, France

[§]CNRS, UMR 7565, F-54506 Vandoeuvre-lès-Nancy, France

[∥]Faculty of Chemistry and Chemical Technology, University of Ljubljana, Aškerčeva c. 5, SI-1000 Ljubljana, Slovenia

[⊥]Biotechnical Faculty, University of Ljubljana, Jamnikarjeva 101, SI-1000 Ljubljana, Slovenia

ABSTRACT: *Aeropyrum pernix* is an aerobic hyperthermophilic archaeon that grows in harsh environmental conditions and as such possesses unique structural and metabolic features. Its membrane interfaces with the extreme environment and is the first line of defense from external factors. Therefore, lipids composing this membrane have special moieties that increase its stability. The membrane of *A. pernix* is composed predominantly of two polar lipids 2,3-di-*O*-sesterterpanyl-*sn*-glicerol-1-phospho-1′(2′-*O*-α-D-glucosyl)-*myo*-inositol (AGI) and 2,3-di-*O*-sesterterpanyl-*sn*-glicerol-1-phospho-*myo*-inositol (AI). Both have methyl branches in their lipid tails and ether linkages and carbohydrates in their headgroup. These moieties significantly affect the structure and dynamics of the bilayer. To provide a molecular level insight into these characteristics, we used here Molecular Dynamics (MD) simulations of lipid bilayers of composition similar to those of the archaeal membranes. First, we show that the electron density profiles along the normal to the bilayers derived from the simulations are in good agreement with the profiles obtained by the small-angle X-ray scattering (SAXS) technique, which provides confidence in the force fields used. Analyses of the simulation data show that the archaeal lipid bilayers are less hydrated than conventional phosphatidylcholine (PC) lipids and that their structure is not affected by the salt present in the surrounding solution. Furthermore, the lateral pressure in their hydrophobic core, due to the presence of the branched tails, is much higher than that at PC-based lipid bilayers. Both the methyl branched tails and the special headgroup moieties contribute to slow drastically the lateral diffusion of the lipids. Furthermore, we found that the lipid head groups associate via hydrogen bonding, which affects their reorientational dynamics. All together, our data provide links between the microscopic properties of these membranes and their overall stability in harsh environments.

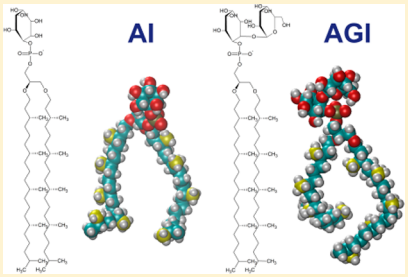

1. INTRODUCTION

Archaea are microorganisms that survive and grow at harsh environmental conditions and as such possess unique structural and metabolic features. They can be grouped on the basis of the extreme environmental conditions as follows: into halophiles that grow in high salt concentration, acidophiles that grow at low pH, alcalophiles that grow at high pH, thermophiles that grow at high temperatures, psychrophilic that grow at low temperatures, and many others.[1−3] The membranes of archaea cells interface with the extreme environment and are the first line of defense against external factors. Therefore, archaeal lipids that form these membranes have special moieties that increase their stability. They are composed in general by glycerophosphate head groups, ether linkages between glycerol moiety and hydrocarbon tails, methyl branching of hydrocarbon chains or hydrocarbon chains with cyclopentane rings, and sometimes are rather bipolar lipids with tetraether core and headgroup composed of carbohydrates.[2]

Aeropyrum pernix K1 is an aerobic hyperthermophilic archaea that grows in a coastal solfataric vent at Kodakara, Juma Island, Japan. It can live in temperatures up to 100 °C. The optimal growth conditions of *A. pernix* are temperature between 90 and 95 °C, pH 7.0, and salinity of 3.5%. The shape of the cells is spherical with a diameter from 0.8 to 1.2 μm.[4] The membranes of these archaea are composed of two lipids: 2,3-di-*O*-sesterterpanyl-*sn*-glicerol-1-phospho-1′(2′-*O*-α-D-glucosyl)-*myo*-inositol (AGI) and 2,3-di-*O*-sesterterpanyl-*sn*-glicerol-1-phospho-*myo*-inositol (AI) with molar ratio of AI and AGI as 9:91 mol %.[5] It has been shown that vesicles composed of AI and AGI lipids are very stable, capable of encapsulating potential substances, and may be uptaken into cells endocytotically.[6,7] It was also found that these lipids are nontoxic to CACO-2 and Hep G2 cells, only mildly toxic to B1-6F1 and CHO cells, and very toxic to EA.hy926 cells.[7]

In this Article, we investigate the structural properties of archaeal lipid bilayer, composed of polar lipids isolated from *A. pernix*, at different temperatures. The bilayers were first investigated using the small-angle X-ray scattering (SAXS) technique, which provided corresponding thickness pair-distance

Received: April 14, 2014
Revised: June 20, 2014
Published: June 25, 2014

   dx.doi.org/10.1021/la5014208 | *Langmuir* 2014, 30, 8308−8315

distribution functions and the electron density profiles. These were then compared to the electron density profiles derived from MD simulations. From the equilibrated bilayers in the MD simulation, we fully characterized the structural and electrostatic properties of these bilayers. This study is an extension of our previous study entitled "Electroporation of Archaeal Lipid Membranes using MD Simulations".[8]

2. MATERIALS AND METHODS

2.1. Growth of *Aeropyrum pernix* K1. *A. pernix* was grown in a 1 L flask at 92 °C. The maximal biomass was obtained by adding $Na_2S_2O_3 \times 5H_2O$ (1 g of per liter) (Alkaloid, Skopje, Macedonia) to Marine Broth 2216 (Difco, Becton, Dickinson and Co., Sparks, U.S.) at pH 7.0 (20 mM HEPES buffer) as described before.[9] After growth, the cells were harvested by centrifugation, washed, and lyophilized.

2.2. Isolation and Purification of Lipids, and Vesicle Preparation. The total polar lipid methanol fraction composed of 91 mol % AGI and 9 mol % AI[5] (average molecular mass, 1181.42 g mol^{-1}) was purified from lyophilized *A. pernix* cells, as described previously.[6] After isolation, the lipids were fractionated with adsorption chromatography.[10] The liposomes were prepared by thin lipid film formation by drying the lipid sample on a rotary evaporator. The dried lipid films were then hydrated by 20 mM HEPES buffer pH 7.0 or deionized water (Milli-Q), temperature 45 °C. Multilamellar vesicles (MLV) were prepared by vortexing the lipid suspensions vigorously for 10 min. MLV were further transformed into large unilamellar vesicles (LUV) by six freeze (liquid nitrogen) and thaw (warm water) cycles and by pressure-extruded 21 times through 400 nm polycarbonate membranes on an Avanti polar mini-extruder (Avanti Polar Lipids, Alabastr, AL), at temperature between 50 and 60 °C. The lipid concentration in the samples for SAXS experiments was 10 mg/mL.

2.3. Small-Angle X-ray Scattering (SAXS) Measurements. SAXS measurements were performed on the modified Kratky compact camera (Anton Paar KG, Graz, Austria)[11] equipped with the focusing multilayer optics for X-rays (Osmic, Max-Flux). The camera was attached to a conventional X-ray generator Kristalloflex 760 (Bruker AXS GmbH, Karlsruhe, Germany) with a sealed X-ray tube (Cu K_α X-rays with a wavelength $\lambda = 0.154$ nm) operating at 40 kV and 35 mA. The samples were measured in a standard quartz capillary with an outer diameter of 1 mm and wall thickness of 10 μm. Position-sensitive detector PSD-50 M (M. Braun GmbH, Garching, Germany) was used for detection of the scattered x-rays in the small-angle regime of scattering vectors $0.1 < q < 7.5$ nm^{-1}, where, $q = 4\pi/\gamma \cdot \sin(\vartheta/2)$, ϑ representing the scattering angle. To get sufficient measuring statistics, each sample was measured for a period of 20 h. Prior to the detailed data analysis, the scattering data were corrected for the empty capillary and solvent scattering, and put on the absolute scale using water as a secondary standard.[12]

2.4. Evaluation of SAXS Data. Experimental SAXS data were evaluated utilizing the Generalized Indirect Fourier Transformation (GIFT) software package.[13−18] There were no interlamellar interference peaks observed in the scattering curves in our case. Similarly, the maximum dimension of the scattering particles (large unilamellar vesicles) was much bigger than the size resolution of the SAXS method; therefore, solely the basic part of the GIFT, that is, the Indirect Fourier Transformation (IFT) technique, was used.[19,20] In such cases, one can still extract the structural information on the thickness of the lipid bilayer from the scattering curves, because the thickness of the bilayer is usually still well within the experimental resolution of the SAXS method. For this purpose, the IFT technique is used in a special mode, where $I(q)q^2$ is cosine transformed into the real space yielding the thickness pair distance distribution function $p_t(r)$.[20−22] In this procedure, a considerable cutoff must be applied to the scattering curves in the regime of very low q values to exclude the part of the scattering curve that is strongly affected by the scattering contribution originating from the large dimensions of the lipid bilayer; in this way, solely the structural information related to the thickness of the lamellar bilayer can be extracted. Such an approach is based on the thickness form factor, $I_t(q)$, which represents the scattering due to the structure in perspective of the bilayer thickness and is completely model-free. The thickness form factor can be written as the cosine transformation of the thickness pair-distance distribution function $p_t(r)$:[20−22]

$$I(q)q^2 = 2\pi A I_t(q) = 4\pi A \int_0^\infty p_t(r)\cos(qr)\,dr \quad (1)$$

where r is the distance between two scattering centers within the particle. The resulting $p_t(r)$ function serves as a tool for the determination of the scattering particles geometry.[19−23] At distances r bigger than the thickness of the bilayer, the $p_t(r)$ function adopts the value of zero and in this way provides a useful tool for the determination of the bilayer thickness. In addition, the scattering contrast profile across the bilayer in direction perpendicular to its plane, which provides valuable information on the bilayer internal structure, can be calculated from the $p_t(r)$ function by a convolution square root operation utilizing the DECON program:[24−26]

$$p_t(r) = \int_{-\infty}^{\infty} \Delta\rho_e(z)\cdot\Delta\rho_e(z - r)\,dr \quad (2)$$

with $\Delta\rho_e(z)$ representing the local scattering contrast, that is, the difference between the local electron density at distance z from the center of symmetry (central plane in the middle of bilayer) and the average electron density of the sample $\overline{\rho}_e$. To facilitate comparison of MD and SAXS results, in further text the scattering contrast profile $\rho_e(z)$ will be referred to simply as the electron density profile and denoted with the symbol $\rho_e(z)$. Note that r in $p_t(r)$ corresponds to the distance in real space (information on the overall bilayer thickness), but z in the electron density profile is determined with respect to the central plane of the bilayer.

2.5. MD Simulations. The molecular dynamics (MD) models and simulations were adopted from our previous study.[8] The MD simulations presented here were carried out using the program NAMD.[27] The systems were examined in the NPT (constant number of atoms, pressure, and temperature) ensembles employing Langevin dynamics and the Langevin piston method. The time step for integrating the equations of motion was set at 2.0 fs. Short- and long-range forces were calculated every one and two time steps, respectively. Bonds between hydrogen and heavy atoms were constrained to their equilibrium value. Long-range, electrostatic forces were taken into account using the particle mash Ewald (PME) approach.[28,29] The structures of AI and AGI molecules, which compose the membrane of *A. pernix*, were suggested by Morii et al.[5] The MD models were built by combining the CHARMM 36 lipid force field and the CHARMM 36 carbohydrate force field. The parameters for ester linkages were adopted from Shinoda et al.[30]

First, the bilayer was composed of 64 lipids (6 AI and 58 AGI). The composition of the bilayer was a molar ratio of 9:91, which was measured experimentally.[5] The bilayer was surrounded by 10 283 water molecules, 144 potassium (K^+), and 80 chloride (Cl^-) ions (~0.45 M KCl). That system was equilibrated for 120 ns at constant numbers of atoms, constant pressure (1 atm), and constant temperature (50 °C) (NPT). The system then was replicated twice in the X and Y directions of the bilayer plane to afford a large membrane patch and equilibrated again at 90, 70, and 25 °C (NPT) for 30 ns. After the equilibration of systems at 70 and 25 °C, the potassium (K^+) and chloride (Cl^-) ions were removed, and then the counterions (Na^+) were added to neutralize the systems and equilibrated again for the 30 ns. The systems with counterions (Na^+) mimicked the situation during the SAXS experiments. The electron density profiles of these two systems were compared to electron density profiles obtained by experimental SAXS. These SAXS data were measured for the systems containing ~0.45 M KCl.

In all of the simulated systems, the average area per lipid was estimated by dividing the total area of the bilayer by the number of lipids in each leaflet. The thickness of the bilayer was defined as the distance between the two highest peaks of the electron density profile. The positions of these peaks correspond to the location of the lipid phosphate groups in bilayer. The radial distribution functions (RDFs) were calculated using the VMD GofRGUI Plugin. The in-plane lateral diffusion coefficients (D) of the lipids were estimated from the slopes of the mean squared displacements (MSDs) of the center of the molecules in the interval from 5 to 15 ns according to

$$D = \frac{1}{2d}\lim_{t\to\infty}\frac{1}{t}\langle |r(t - t_0) - r(t_0)|^2\rangle_z \quad (3)$$

dx.doi.org/10.1021/la5014208 | Langmuir 2014, 30, 8308−8315

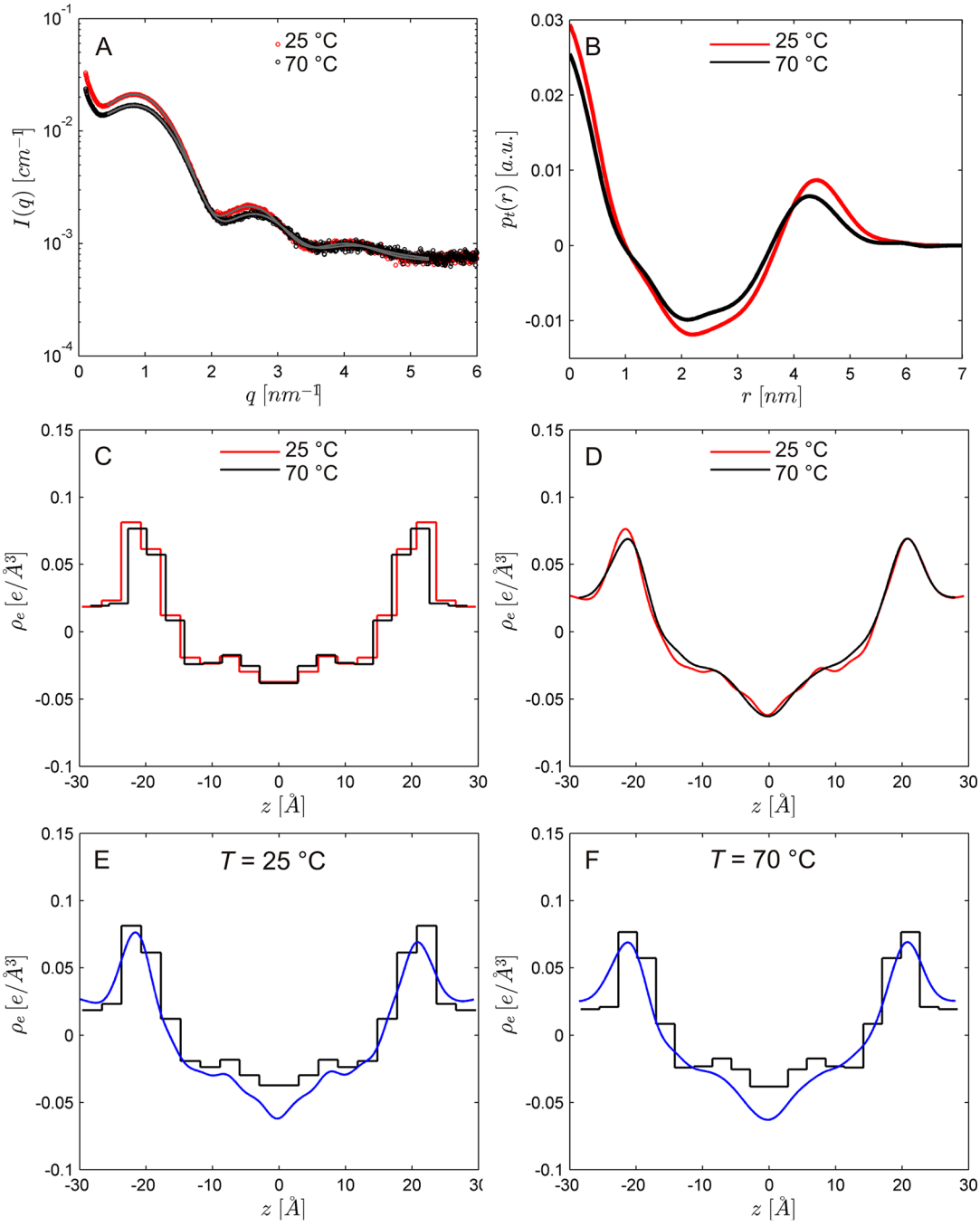

Figure 1. (A) Experimental SAXS curves of liposomes composed of archaeal lipids at 25 °C (red ○) and 70 °C (○) on absolute scale and IFT fits for the lamellar symmetry (gray lines). (B) The corresponding results of the IFT evaluation for lamellar symmetry−thickness pair-distance distribution functions $p_t(r)$. (C) Electron density profiles $\rho_e(z)$ determined on the basis of the experimental SAXS results obtained from the $p_t(r)$ functions by a convolution square root operation. (D) Electron density profiles of archaeal lipid bilayers derived from MD simulations. The electron density profiles of liposomes composed of archaeal lipids at 25 °C (E) and 70 °C (F). The profiles are derived from MD simulations (archaeal lipids in water with counterions Na^+) (blue) and electron density profiles $\rho_e(z)$ determined on the basis of the experimental SAXS results (black). These comparisons of electron density profiles between SAXS measurements and MD simulations have already been published by Polak et al.[8]

where $d = 2$ is the number of translational degrees of freedom and $t_0 = 5$ ns.

The rotational motion of the head groups moieties was calculated using the second rank reorientational autocorrelation function:

$$C(t) = \frac{1}{2}\langle 3[\vec{V}(t)\cdot\vec{V}(0)]^2 - 1\rangle \quad (4)$$

where **V** is unit vector defined in Figure 5A.

All tof he analyses were performed on the data of the last 15 ns of each simulation run.

We have also estimated the local pressure profiles[31] along z, the bilayer normal, at various system configurations. The pressure profiles may be calculated from simulations as

$$p(z) = \frac{1}{\Delta V}[\sum_i m_i \mathbf{v}_i \otimes \mathbf{v}_i - \sum_{i<j} \mathbf{F}_{ij} \otimes \mathbf{r}_{ij} f(z, z_i, z_j)] \quad (5)$$

where $p(z)$ is the local pressure tensor in the slab centered on the coordinate z, the sum over the kinetic term running over all atoms in the slab, and $f(z,z_i,z_j)$ is a weighting function. The calculations were all

dx.doi.org/10.1021/la5014208 | *Langmuir* 2014, 30, 8308−8315

performed on the fly[27] from the simulations performed at constant temperature and constant pressure. The lateral pressure profiles were calculated using built-in function in NAMD. The simulation space is partitioned into slabs, and one-half of the virial due to the interaction between two particles is assigned to each of the slabs containing the particles. To evaluate local pressure, the Harasima contour was used. The algorithm is based on that of Lindahl and Edholm,[32] with modifications to enable Ewald sums based on Sonne et al.[33] The total virial contains contributions from kinetic energy, bonded interactions, nonbonded interactions, and an Ewald sum. In lipid bilayers, the pressure profiles arise due to the amphipathic nature of the lipids composing it: the hydrophilic head groups are squeezed together to prevent exposure of the hydrophobic tails to the solvent leading to a negative lateral pressure, while the attractive dispersion forces and entropic repulsion between the lipid tails result mainly in a positive lateral pressure.

3. RESULTS AND DISCUSSION

The experimental SAXS curves of the vesicle sample composed of archaeal lipids at 25 and 70 °C are depicted in Figure 1A. These scattering curves show three broad scattering peaks that are increasing in intensity with decreasing scattering vector q and a steep upturn of the scattering intensity at very low values of q. The broad scattering peaks occur in the q region corresponding to the thickness of the lipid bilayer, whereas the steep upturn at very low values of q occurs due to the very large overall dimensions of the bilayer that are above the resolution of the SAXS experiment. As the temperature increases, the broad scattering peaks decrease in intensity and shift toward higher q values. This indicates an increase in the bilayer thickness, which possibly leads also to a slight change in the scattering contrast of the bilayer.

Because of the limited experimental resolution, the information on the overall size of the vesicles is not complete in these SAXS results; therefore, the steep upturn at low q needs to be cut off before the detailed IFT evaluation of the SAXS data containing information on the internal structure of the bilayer. The fits obtained by the IFT analysis are shown as gray lines in Figure 1A, whereas the resulting thickness pair-distance distribution functions $p_t(r)$ are depicted in Figure 1B. These functions reveal a rather similar internal structure of these bilayers in terms of the scattering contrast, with somewhat larger overall thicknesses of the bilayer at lower temperature (6 nm at 25 °C vs 5.5 nm at 70 °C). At higher temperature, the thermal energy of lipid molecules is higher; the hydrophobic tails become more flexible and hydrophobic heads are hydrated to a lesser extent, and so therefore the lipid molecules can obviously pack themselves into thinner bilayers.

The internal structure of the lipid bilayers is revealed in more detail through the electron density profiles. These profiles were obtained via convolution square root procedure of the experimentally obtained $p_t(r)$ functions and also by the MD simulations. The electron density profiles obtained by MD and SAXS method at 25 and 70 °C are shown in Figure 1. These profiles show that the central part of the bilayer is negative, whereas the outer layers have the positive electron density in comparison to the average electron density of the sample; the latter defines $\rho_e = 0$. This is in agreement with the lower electron density of the hydrophobic hydrocarbon parts of the lipid molecules (comprising the central part of the lipid bilayer) in comparison to the higher electron density of the polar headgroup parts of the lipid molecules (comprising the outer shells on each side of the bilayer). They also reveal the approximate thickness of the central hydrophobic part (~3 nm) and the outer hydrophilic shells of the bilayer (~1.5 nm) and their slight changes with the temperature. The comparison of the MD electron density profiles of the bilayers in two different buffers shows (water with counterions (Na+) and 0.45 M KCl) that the buffer has practically no effect on the electron density profile of the bilayer (data not shown). The shift in positions of the $\rho_e(z)$ peaks that is observed with the temperature increase corresponds to the changes in the outer shells in the bilayers increases. Figure 1 also shows that the bilayers at lower temperatures are somewhat thicker.

The comparison of electron density profiles derived from MD simulations and SAXS results shows a good agreement. Slight discrepancies in the absolute values of $\rho_e(z)$ can be noticed (Figure 1). These can arise either from the different nature of the two techniques, from the numerical model of the system itself, or from impurities in the real samples that cannot be taken into account in the simulations. Nevertheless, these results confirm the structural accuracy of the model and the force field used in our study.

The time evolutions of the surface area per molecule (A_m) for archaeal lipid in water with the Na^+ counterions and in the 0.45 M KCl solution at different temperatures show that the bilayers were well equilibrated within few tens of nanosecond (data not shown). The values of A_m and of the bilayer thickness (phosphates peak-to-peak distance) are reported in Table 1.

Table 1. Properties of the Equilibrated Archaeal Lipid Bilayers in Different Buffers and at Different Temperatures from MD Simulations[a]

buffer	T [°C]	A_m [Å^2]	d [Å]
Na^+ counterions	25	83.4 ± 0.4	42.5
	70	86.7 ± 0.7	42.1
0.45 M KCl	25	82.5 ± 0.3	42.5
	70	86.8 ± 0.6	42.1
	90	90.4 ± 0.7	41.8

[a] T, temperature; A_m, area per molecule; d, thickness of the bilayer.

As expected, they increase and decrease, respectively, with increasing temperature. Again, we found that the presence of buffer in the systems has practically no effect on A_m. Shinoda et al.[34] showed that the concentration of NaCl does not affect the structure of DPhPC-ether. This supports our findings of archaeal lipids. On the other hand, Knecht and Klasczyk[35] suggest that chloride ions bind almost as strongly to PC bilayers as sodium ions, and they do not affect the structure of bilayer. This was calculated by experiments and compared to molecular dynamic simulations. They are suggesting that a range of published simulation results on the interaction of NaCl with PC bilayers have to be reconsidered and revised.

To further characterize the systems under study, we derived from the MD simulations the density profiles of the bilayers main components across the membrane normal. The potassium ions penetrate more deeply into the bilayer as compared to the chloride ions, which is expected due to the negative charges carried by the lipid head groups. Quite interestingly, the same components of the AI and AGI molecules (lipid hydrocarbon tails, glycerol, phosphate, inositol, and glucose moieties) have similar distributions along the bilayer normal, although the AGI molecules carry an additional glucose group. The latter partition in the region of phosphate and inositol groups and are indicated by a broader density distribution pointing to its high mobility and conformational freedom.

dx.doi.org/10.1021/la5014208 | Langmuir 2014, 30, 8308−8315

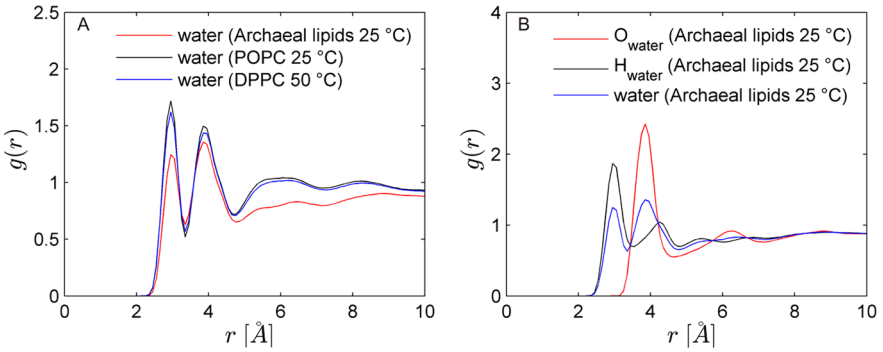

Figure 2. Radial distribution functions (RDFs).

The average location of the lipid components with respect to the solvent indicates that hydration of the head groups in these lipids is quite different from that in simple lipid bilayers. To characterize the latter, we have measured the radial distribution functions (RDF) of the solvent (water molecules) around the phosphorus atom in the archaeal lipids (Figure 2) and that of POPC and DPPC bilayers for the purpose of comparison. The data show that there is hardly any difference between these distribution functions for the two PC-based lipids, but a large one between PC and archaeal lipids. Furthermore, the RDFs at 70 and 90 °C are exactly the same (data not shown). Table 2 reports

Table 2. Coordinate Number, the Number of Atoms in the First Shell around Phosphorous Atom in Archaeal Lipids, POPC, and DPPC

	coordination number		
atom pair	archaeal lipid	POPC	DPPC
P–H_{water}	4.60	5.87	5.64
P–O_{water}	5.64	5.98	5.98
P–water	3.98	5.45	5.20

the coordination numbers and indicates that the phosphorus head groups in archaeal lipid are indeed less hydrated than those in PC-based lipid bilayers.

Interactions between the lipid components probably play a major role in the stability of the bilayer. They moreover slow the overall dynamics of the lipid head groups as well as the lateral diffusion of the lipids, as we further quantify in the following paragraphs. Because of the difference in interactions between the headgroup moieties and the tails, one expects also a difference in the pressure profiles along the membrane normal for these archaeal and simple PC-based lipids with acyl chains. These profiles have been calculated and are reported together with those of POPC and DPPC bilayer in Figure 3. Aside from a difference due to the change in bilayer hydrophobic core thickness, the peaks of the pressure at the interfacial regions are much higher in archaeal lipids as compared to PC-based lipids. As it was observed, the archaeal lipid bilayers have a much larger positive lateral pressure in the hydrophobic region.

Turning back to the dynamical characteristics of the archaeal lipid bilayer, we estimated the molecules lateral diffusion coefficients D from the MSD curves by linear fitting (Figure 4). They indicate that archaeal lipids have much lower lateral diffusion than other phosphatidylcholine (PC) lipids at temperatures above the gel to liquid crystal phase transitions. For instance, the lateral diffusion coefficients of DPPC lipids (measured experimentally or estimated from MD simulations) amount to

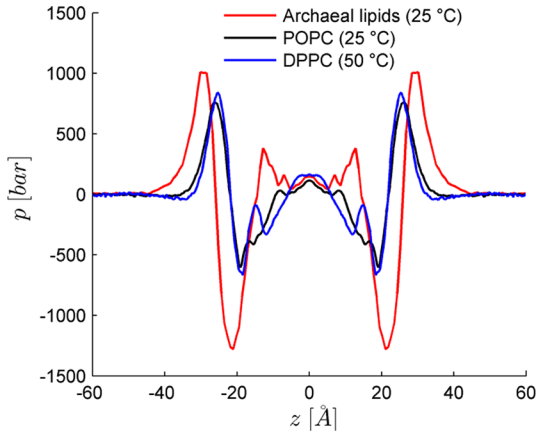

Figure 3. Lateral pressure profile of archaeal lipid (red), POPC (black), and DPPC (blue) bilayers.

~1–4 × 10^{-7} cm^2/s,[36–38] and for 1,2-diphytanoyl-*sn*-glycero-3-phosphocholine (DPhPC)-ether at 25 °C D is ~4.8 × 10^{-8} cm^2/s.[39]

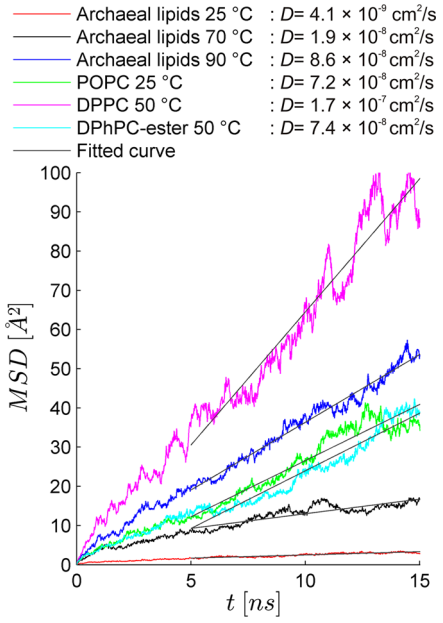

Figure 4. Mean square displacement (MSD) of lipids in the bilayer composed of archaeal lipids, POPC, and DPPC. The gray linear curves are fitted curves to the data from 5 to 15 ns. From fitted curves was the diffusion coefficient (D) calculated. The D values of POPC, DPPC, and DPhPC-ester were determined on our unpublished and published MD system.[40]

dx.doi.org/10.1021/la5014208 | *Langmuir* 2014, 30, 8308–8315

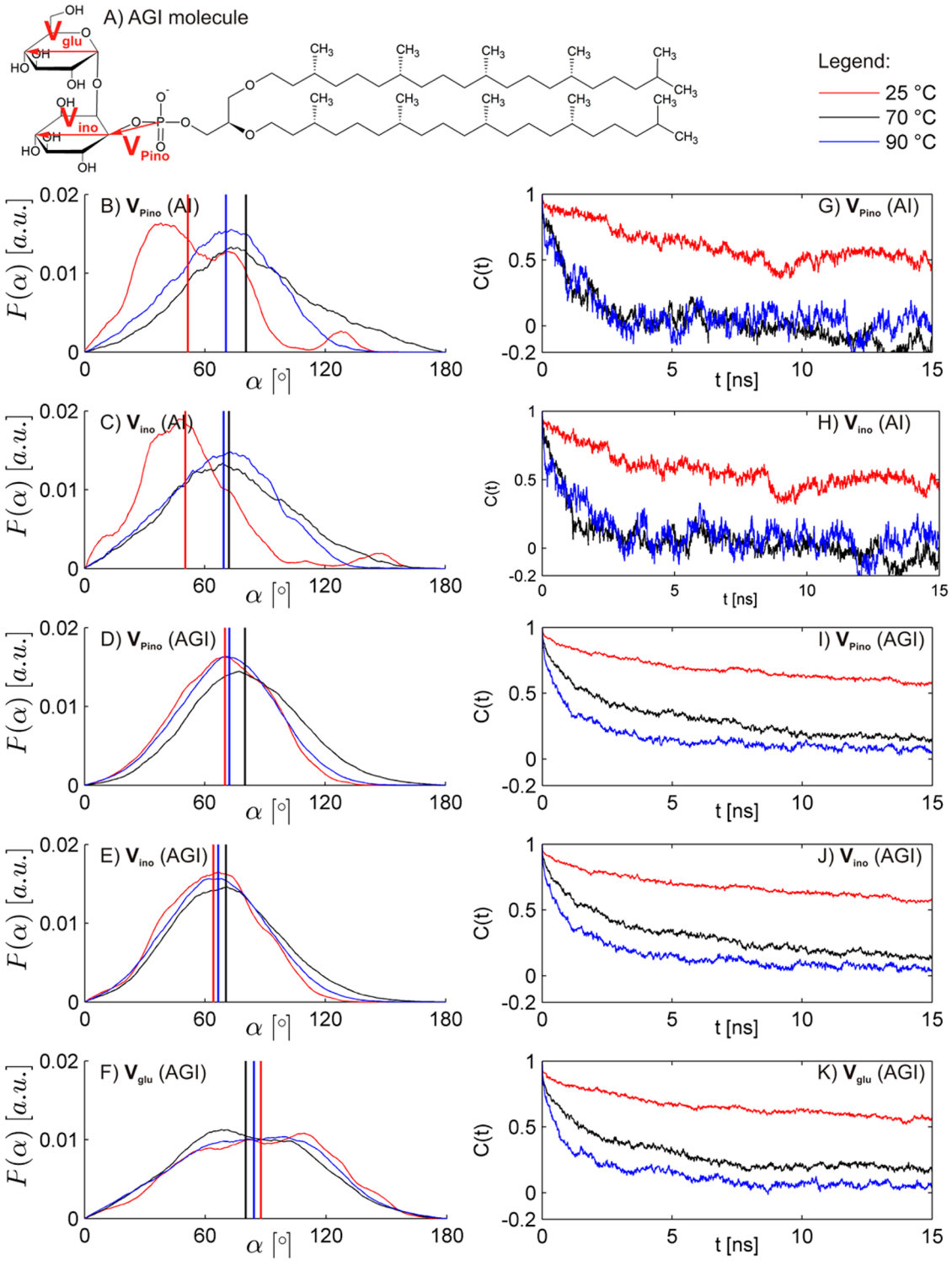

Figure 5. (A) AGI molecule with labeled vectors in the headgroup. The distributions of angle (α) between $\mathbf{V}_{Pino}$, $\mathbf{V}_{ino}$, and $\mathbf{V}_{glu}$, and normal to archaeal lipid bilayers at 25, 70, and 90 °C (B–F). Vertical lines represent the median value of α. The graphs G–K present the reorientation autocorrelation function $C(t)$. The data are derived from MD simulations.

Figure 5 shows the orientations and reorientation autocorrelation functions of the archaeal lipid headgroup components with respect to the bilayer normal. We introduce here several vectors along these head groups to characterize the conformation of the lipids: $\mathbf{V}_{Pino}$ pointing from the phosphorus atom to the C-1 atom of inositol, $\mathbf{V}_{ino}$ pointing from C-1 to C-4 atoms of the inositol (representing the orientation of the inositol), and $\mathbf{V}_{glu}$ pointing from C-1 to C-4 of the glucose (representing the orientation of glucose group) (Figure 5A). As the angles are not normally distributed, we calculated median values of angles between vectors (Figure 5 and Table 3). We notice small differences in the distribution of $\mathbf{V}_{Pino}$ and $\mathbf{V}_{ino}$ in AGI molecules at different temperatures. The $\mathbf{V}_{Pino}$ and $\mathbf{V}_{ino}$ in AI molecules have similar distributions at 70 and 90 °C. At 25 °C, there is a large change in

dx.doi.org/10.1021/la5014208 | Langmuir 2014, 30, 8308–8315

Table 3. Median Values of Angle (α) between V_{Pino}, V_{ino}, and V_{glu}, and Normal to Archaeal Lipid Bilayers Composed of AI and AGI Molecules and Half Time Constant of Reorientation Autocorrelation Function ($\tau_{1/2}$) at 25, 70, and 90 °C

		25 °C		70 °C		90 °C	
vector	molecule	α [deg]	$\tau_{1/2}$ [ns]	α [deg]	$\tau_{1/2}$ [ns]	α [deg]	$\tau_{1/2}$ [ns]
V_{Pino}	AI	51.5	7.51	80.5	0.69	70.5	0.50
V_{Pino}	AGI	70.1	–	80.1	1.78	72.3	0.60
V_{ino}	AI	50.4	5.54	72.1	0.75	69.5	0.19
V_{ino}	AGI	64.2	–	70.5	1.94	66.5	0.69
V_{glu}	AGI	87.6	–	80.1	1.40	84.2	0.58

the conformation of the AI headgroup. It flips to almost perpendicular orientation with respect to the bilayer plane. The glucose in the headgroup has a bimodal distribution. This means that the latter are tilted into or out of the bilayer. The reorientational autocorrelation functions provide insight into the dynamics of the lipid head groups (Figure 5G, I, J, K). As expected, the time constants of the auto correlation decay are higher for larger temperatures, but we also observe that headgroup moieties of AI lipids are moving faster than the headgroup moieties of AGI lipids. The presence of glucose in the AGI molecule appears to lower the dynamic of the headgroup moieties, probably due to the formation of hydrogen bonds with surrounding headgroup moieties. In comparison to simple PC-based lipids (e.g., DPPC), the dynamic of V_{Pino} reorientation even at 90 °C is much slower than the dynamics of P−N vector estimated at 50 °C ($\tau_{1/2}$ = 0.3 ns).[41]

4. SUMMARY AND CONCLUSIONS

The *Aeropyrum pernix* is a rare cell organism, whose membrane is composed predominantly of two polar lipids (AI and AGI). There is no report whether the AI and AGI molecules are randomly distributed or aggregate in the membrane of *A. pernix*. Accordingly, in this study, we modeled archaeal lipid bilayers assuming a random distribution of its components. The bilayers were simulated at a wide range of temperatures and at different salt concentrations. We considered in particular temperatures where the archaeal lipid bilayers are in the liquid crystalline phase. For comparison, DPhPC phospholipids that carry methyl groups in lipid tails as do AI and AGI lipids[2] are also liquid crystalline in a wide range of temperatures (−120 and 120 °C).[42] The structural properties of AI and AGI bilayers were calculated and compared to electron density profiles extracted from SAXS measurements. The agreement obtained provided confidence in the force field parameters and protocols used in the MD simulations.

The properties of the archaeal bilayers as the average area per lipid, the hydrophobic core thickness, the orientation of the lipid head-groups, and the dynamics of the lipids significantly change with temperature in the range studied here (25−90 °C), while the salt nature and content seem to have no effect on the structure of the bilayer (area per lipid and thickness). The presence of salt seems also to have a negligible effect on the bilayer structure as the archaeal lipids associate through hydrogen bonding between their headgroup moieties. As compared to PC-based lipid bilayers, the archaeal lipids head groups are less hydrated than PC-based lipids.

The in-plane dynamics of the archaeal lipids in the bilayers is much slower than that of other PC-based lipids. The lateral diffusion coefficient (D) of AI and AGI lipids is indeed lower than that of other PC-based lipids, even when comparing archaeal bilayers at 90 °C and PC-based bilayers at 25 °C. The slower dynamics is in part due the methyl-branches in the lipid tails,[39] but, more importantly, due to the large sugar moieties of the lipid head groups. Inositol and glucose indeed interact with each other through hydrogen bonding. The orientation of the headgroup moieties is quite similar at all temperatures studied with the exception of that of the AI molecule at 25 °C. The glucose in AGI molecules has a bimodal distribution (facing inward and outward the bilayer plane). The dynamics of the headgroup moieties described by reorientational correlation functions is faster at the higher temperatures studied. Furthermore, this headgroup dynamics is faster for the AI head groups, as compared to AGI, as the former are not only smaller, but lack the glucose groups that form stable hydrogen bonds with neighboring lipids.

The lateral pressure profile of archaeal lipid bilayers also shows significant differences from that of PC-based lipid bilayers. In particular, the lateral pressure in the hydrophobic core is much higher, and the negative pressure due mainly to attractive forces just beneath the head groups is also much higher. The surface tension of bilayers that corresponds to the integral of the pressure profile along the bilayer is important for the function of membrane proteins and determines in general the elastic properties of lipid bilayers.[43] The differences highlighted here, between simple PC-based lipids and archaeal lipids, relate directly to their interesting and unusual physical properties.

AUTHOR INFORMATION

Corresponding Authors

*E-mail: mounir.tarek@univ-lorraine.fr.

*Tel.: +386-14-768-456. E-mail: damijan.miklavcic@fe.uni-lj.si.

Notes

The authors declare no competing financial interest.

ACKNOWLEDGMENTS

This research was conducted within the scope of the EBAM European Associated Laboratory. This work was in part supported by the Slovenian Research Agency (J2-3639, P1-0201, P2-0249, and P4-0121). This manuscript is a result of the networking efforts of COST Action TD1104 (www.electroporation.net). Part of the calculations of the paper was performed during the Short Term Scientific Mission Grant STSM [070113-021794] to A.P. Simulations were performed using HPC resources from GENCI-CINES (Grant 2012−2013 [076434]).

REFERENCES

(1) Benvegnu, T.; Brard, M.; Plusquellec, D. Archaeabacteria Bipolar Lipid Analogues: Structure, Synthesis and Lyotropic Properties. *Curr. Opin. Colloid Interface Sci.* **2004**, *8*, 469−479.

(2) Ulrih, N. P.; Gmajner, D.; Raspor, P. Structural and Physicochemical Properties of Polar Lipids from Thermophilic Archaea. *Appl. Microbiol. Biotechnol.* **2009**, *84*, 249−260.

(3) Ulrih, N. P.; Adamlje, U.; Nemec, M.; Sentjurc, M. Temperature- and pH-Induced Structural Changes in the Membrane of the

Hyperthermophilic Archaeon Aeropyrum Pernix K1. *J. Membr. Biol.* **2007**, *219*, 1−8.
(4) Sako, Y.; Nomura, N.; Uchida, A.; Ishida, Y.; Morii, H.; Koga, Y.; Hoaki, T.; Maruyama, T. Aeropyrum Pernix Gen. Nov., Sp. Nov., a Novel Aerobic Hyperthermophilic Archaeon Growing at Temperatures up to 100°C. *Int. J. Syst. Bacteriol.* **1996**, *46*, 1070−1077.
(5) Morii, H.; Yagi, H.; Akutsu, H.; Nomura, N.; Sako, Y.; Koga, Y. A Novel Phosphoglycolipid Archaetidyl(glucosyl)inositol with Two Sesterterpanyl Chains from the Aerobic Hyperthermophilic Archaeon Aeropyrum Pernix K1. *Biochim. Biophys. Acta, Mol. Cell Biol. Lipids* **1999**, *1436*, 426−436.
(6) Gmajner, D.; Ota, A.; Sentjurc, M.; Ulrih, N. P. Stability of Diether C(25,25) Liposomes from the Hyperthermophilic Archaeon Aeropyrum Pernix K1. *Chem. Phys. Lipids* **2011**, *164*, 236−245.
(7) Napotnik, T. B.; Valant, J.; Gmajner, D.; Passamonti, S.; Miklavcic, D.; Ulrih, N. P. Cytotoxicity and Uptake of Archaeosomes Prepared from Aeropyrum Pernix Lipids. *Hum. Exp. Toxicol.* **2013**.
(8) Polak, A.; Tarek, M.; Tomšič, M.; Valant, J.; Ulrih, N. P.; Jamnik, A.; Kramar, P.; Miklavčič, D. Electroporation of Archaeal Lipid Membranes Using MD Simulations. *Bioelectrochemistry* **2014**.
(9) Milek, I.; Cigic, B.; Skrt, M.; Kaletunç, G.; Ulrih, N. P. Optimization of Growth for the Hyperthermophilic Archaeon Aeropyrum Pernix on a Small-Batch Scale. *Can. J. Microbiol.* **2005**, *51*, 805−809.
(10) Bligh, E. G.; Dyer, W. J. A Rapid Method of Total Lipid Extractin and Purification. *Can. J. Biochem. Physiol.* **1959**, *37*, 911−917.
(11) Kratky, O.; Stabinger, H. X-Ray Small Angle Camera with Block-Collimation System an Instrument of Colloid Research. *Colloid Polym. Sci.* **1984**, *262*, 345−360.
(12) Orthaber, D.; Bergmann, A.; Glatter, O. SAXS Experiments on Absolute Scale with Kratky Systems Using Water as a Secondary Standard. *J. Appl. Crystallogr.* **2000**, *33*, 218−225.
(13) Weyerich, B.; Brunner-Popela, J.; Glatter, O. Small-Angle Scattering of Interacting Particles. II. Generalized Indirect Fourier Transformation under Consideration of the Effective Structure Factor for Polydisperse Systems. *J. Appl. Crystallogr.* **1999**, *32*, 197−209.
(14) Brunner-Popela, J.; Mittelbach, R.; Strey, R.; Schubert, K.-V.; Kaler, E. W.; Glatter, O. Small-Angle Scattering of Interacting Particles. III. D[sub 2]O-C[sub 12]E[sub 5] Mixtures and Microemulsions with N-Octane. *J. Chem. Phys.* **1999**, *110*, 10623.
(15) Fritz, G.; Bergmann, A.; Glatter, O. Evaluation of Small-Angle Scattering Data of Charged Particles Using the Generalized Indirect Fourier Transformation Technique. *J. Chem. Phys.* **2000**, *113*, 9733.
(16) Frühwirth, T.; Fritz, G.; Freiberger, N.; Glatter, O. Structure and Order in Lamellar Phases Determined by Small-Angle Scattering. *J. Appl. Crystallogr.* **2004**, *37*, 703−710.
(17) Fritz, G.; Glatter, O. Structure and Interaction in Dense Colloidal Systems: Evaluation of Scattering Data by the Generalized Indirect Fourier Transformation Method. *J. Phys.: Condens. Matter* **2006**, *18*, S2403−S2419.
(18) Glatter, O. The Interpretation of Real-Space Information from Small-Angle Scattering Experiments. *J. Appl. Crystallogr.* **1979**, *12*, 166−175.
(19) Glatter, O. A New Method for the Evaluation of Small-Angle Scattering Data. *J. Appl. Crystallogr.* **1977**, *10*, 415−421.
(20) Glatter, O. Evaluation of Small-Angle Scattering Data from Lamellar and Cylindrical Particles by the Indirect Transformation Method. *J. Appl. Crystallogr.* **1980**, *13*, 577−584.
(21) Iampietro, D. J.; Brasher, L. L.; Kaler, E. W.; Stradner, A.; Glatter, O. Direct Analysis of SANS and SAXS Measurements of Catanionic Surfactant Mixtures by Fourier Transformation. *J. Phys. Chem. B* **1998**, *102*, 3105−3113.
(22) Sato, T.; Sakai, H.; Sou, K.; Medebach, M.; Glatter, O.; Tsuchida, E. Static Structures and Dynamics of Hemoglobin Vesicle (HBV) Developed as a Transfusion Alternative. *J. Phys. Chem. B* **2009**, *113*, 8418−8428.
(23) Glatter, O. In *Small Angle X-ray Scattering*; Glatter, O., Kratky, O., Eds.; Academic Press Inc. London Ltd.: London, 1983; p 119.
(24) Glatter, O. Convolution Square Root of Band-Limited Symmetrical Functions and Its Application to Small-Angle Scattering Data. *J. Appl. Crystallogr.* **1981**, *14*, 101−108.
(25) Glatter, O.; Hainisch, B. Improvements in Real-Space Deconvolution of Small-Angle Scattering Data. *J. Appl. Crystallogr.* **1984**, *17*, 435−441.
(26) Mittelbach, R.; Glatter, O. Direct Structure Analysis of Small-Angle Scattering Data from Polydisperse Colloidal Particles. *J. Appl. Crystallogr.* **1998**, *31*, 600−608.
(27) Kalé, L.; Skeel, R.; Bhandarkar, M.; Brunner, R.; Gursoy, A.; Krawetz, N.; Phillips, J.; Shinozaki, A.; Varadarajan, K.; Schulten, K. NAMD2: Greater Scalability for Parallel Molecular Dynamics. *J. Comput. Phys.* **1999**, *151*, 283−312.
(28) Essmann, U.; Perera, L.; Berkowitz, M. L.; Darden, T.; Lee, H.; Pedersen, L. G. A Smooth Particle Mesh Ewald Method. *J. Chem. Phys.* **1995**, *103*, 8577.
(29) Darden, T.; York, D.; Pedersen, L. Particle Mesh Ewald: An N log(N) Method for Ewald Sums in Large Systems. *J. Chem. Phys.* **1993**, *98*, 10089.
(30) Shinoda, K.; Shinoda, W.; Baba, T.; Mikami, M. Comparative Molecular Dynamics Study of Ether- and Ester-Linked Phospholipid Bilayers. *J. Chem. Phys.* **2004**, *121*, 9648−9654.
(31) Lindahl, E.; Edholm, O. Spatial and Energetic-Entropic Decomposition of Surface Tension in Lipid Bilayers from Molecular Dynamics Simulations. *J. Chem. Phys.* **2000**, *113*, 3882.
(32) Hess, B.; Kutzner, C.; van der Spoel, D.; Lindahl, E. GROMACS 4: Algorithms for Highly Efficient, Load-Balanced, and Scalable Molecular Simulation. *J. Chem. Theory Comput.* **2008**, *4*, 435−447.
(33) Sonne, J.; Hansen, F. Y.; Peters, G. H. Methodological Problems in Pressure Profile Calculations for Lipid Bilayers. *J. Chem. Phys.* **2005**, *122*, 124903.
(34) Shinoda, K.; Shinoda, W.; Mikami, M. Molecular Dynamics Simulation of an Archaeal Lipid Bilayer with Sodium Chloride. *Phys. Chem. Chem. Phys.* **2007**, *9*, 643−650.
(35) Knecht, V.; Klasczyk, B. Specific Binding of Chloride Ions to Lipid Vesicles and Implications at Molecular Scale. *Biophys. J.* **2013**, *104*, 818−824.
(36) Pfeiffer, W.; Henkel, T.; Sackmann, E.; Knoll, W.; Richter, D. Local Dynamics of Lipid Bilayers Studied by Incoherent Quasi-Elastic Neutron Scattering. *Europhys. Lett.* **1989**, *8*, 201−206.
(37) Essmann, U.; Berkowitz, M. L. Dynamical Properties of Phospholipid Bilayers from Computer Simulation. *Biophys. J.* **1999**, *76*, 2081−2089.
(38) Hofsäß, C.; Lindahl, E.; Edholm, O. Molecular Dynamics Simulations of Phospholipid Bilayers with Cholesterol. *Biophys. J.* **2003**, *84*, 2192−2206.
(39) Shinoda, W.; Shinoda, K.; Baba, T.; Mikami, M. Molecular Dynamics Study of Bipolar Tetraether Lipid Membranes. *Biophys. J.* **2005**, *89*, 3195−3202.
(40) Polak, A.; Bonhenry, D.; Dehez, F.; Kramar, P.; Miklavčič, D.; Tarek, M. On the Electroporation Thresholds of Lipid Bilayers: Molecular Dynamics Simulation Investigations. *J. Membr. Biol.* **2013**, *246*, 843−850.
(41) Niemelä, P.; Hyvönen, M. T.; Vattulainen, I. Structure and Dynamics of Sphingomyelin Bilayer: Insight Gained through Systematic Comparison to Phosphatidylcholine. *Biophys. J.* **2004**, *87*, 2976−2989.
(42) Andersson, M.; Jackman, J.; Wilson, D.; Jarvoll, P.; Alfredsson, V.; Okeyo, G.; Duran, R. Vesicle and Bilayer Formation of Diphytanoylphosphatidylcholine (DPhPC) and Diphytanoylphosphatidylethanolamine (DPhPE) Mixtures and Their Bilayers' Electrical Stability. *Colloids Surf., B: Biointerfaces* **2011**, *82*, 550−561.
(43) Ollila, S. Lateral Pressure in Lipid Membranes and Its Role in Function of Membrane Proteins. Ph.D. Thesis, Tampere University of Technology, 2010; p 70.